On the Feasibility of Single-Molecule Detection of the Guanosine-Analogue 3-MI

Jason E. Sanabia,[†] Lori S. Goldner,*,[†] Pierre-Antoine Lacaze,[†] and Mary E. Hawkins[‡]

Optical Technology Division, National Institute of Standards and Technology, Gaithersburg, Maryland 20899 and Pediatric Oncology Branch, National Cancer Institute, Bethesda, Maryland 20892

We present UV fluorescence fluctuation correlation spectroscopy (FCS) measurements on the guanosine-analogue 3-MI [3-methyl-8-(2-deoxy-β-D-ribofuranosyl)isoxanthopterin], a pteridine widely used in studies of DNA binding and dynamics. We measure the photon count rate and signal-to-background ratio per molecule, for both monomeric 3-MI and a 3-MI-containing oligonucleotide. For the monomer, we find a maximum photon count rate per molecule above 4 kHz and a maximum signal-to-background ratio of 5. For incorporated 3-MI, both parameters are a factor of 4 smaller. We discuss the triplet and photobleaching behavior of 3-MI and the possibilities of using this analogue in single-molecule studies of DNA dynamics. Comparisons are made to the behavior of stilbene 3, a brilliant laser dye with a similar fluorescence spectrum.

1. Introduction

Nucleic acid analogues offer an attractive alternative to the use of linker-attached dyes in the study of DNA binding and dynamics. For bulk assays, analogues are widely exploited as a way to avoid artifacts associated with linker and dye structure and dynamics (for a review, see ref 1). For single-molecule studies, the use of analogues has been thwarted by their smaller absorption cross sections, absorption maxima that tend to be in the UV, and a propensity to photobleach. Here, we investigate the potential of 3-MI [3-methyl-8-(2-deoxy-β-D-ribofuranosyl)-isoxanthopterin], a guanosine analogue,[2] in the study of single DNA molecules. We show that single-molecule detection of 3-MI monomer is possible and suggest that single-molecule spectroscopic techniques can successfully be applied to DNA incorporated with 3-MI.

Nucleoside analogues offer some advantages over labeling with a linker-attached chromophore. Because of their size and shape, nucleoside analogues may be incorporated directly into DNA as a replacement for a particular base (see Figure 1). This greatly simplifies attachment chemistry and purification, because they can be incorporated using automated DNA synthesis. The intimate association between the pteridine analogue and the neighboring bases in a sequence has a direct and sequence-dependent effect on the fluorescence properties of the analogues.[2-4] Observing these effects provides a means of monitoring even subtle changes in the strand as it meets and reacts with other molecules. Another very important feature of these analogues is that artifacts caused by chromophore and tether dynamics are greatly reduced. Deprez et al.[5] have demonstrated that the use of the analogue, 3-MI, results in narrower rotational correlation time distributions as compared to the use of fluorescein attached by a six-carbon linker. Hill and Royer[6] have determined through measurements of time-resolved anisotropy that only about 15% of C6-linker-attached fluorescein molecules are coupled to the global tumbling of the DNA.

Single-molecule detection requires that chromophores be extremely bright to overcome background, and stable against
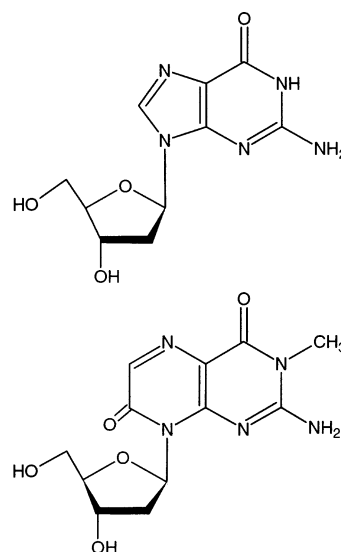
Figure 1. Top: Guanosine. Bottom: 3-MI.

photobleaching. Previously tested nucleic acid analogues have not been exploited in the study of single DNA molecules, in large part because their absorbance tends to be in the UV, where both background and photobleaching problems are exacerbated. Wennmalm et al.[7] characterized 2-aminopurine (2-AP, an adenosine analogue with an absorbance maximum at 300 nm) using methods similar to those employed here. While the number of fluorescent photon counts per second per molecule was approximately 2 kHz, well above the dark count of modern detectors, the signal-to-background ratio was only 0.3 for single-molecule detection. We demonstrate a signal-to-background ratio for 3-MI (absorbance maximum at 350 nm) more than an order of magnitude higher, at least in part due to the longer excitation wavelength of 3-MI as compared to 2-AP. Another problem common with UV fluorophores is their propensity to photobleach. In the study of proteins, tryptophan is widely used as a native fluorescent indicator. Lippitz et al.[8] reported that, for two-photon (590 nm) excitation of tryptophan, photobleaching limited the number of emitted photons per tryptophan molecule to only 2. From data reported here, taken

---

* Corresponding author. E-mail: lori.goldner@nist.gov.
† National Institute of Standards and Technology.
‡ National Cancer Institute.

in the absence of any effort to limit the amount of oxygen present and with one photon excitation, we find an average number of detectable photons before photobleaching for 3-MI to be 395.

3-MI is a pteridine-based fluorescent guanosine analogue (Figure 1) with a quantum yield of 0.88 (in monomer form), an absorbance maximum at 350 nm, an emission maximum at 430 nm, and a reputation for being chemically robust as well as photostable.[2] Quenching of 3-MI incorporated into DNA is caused mostly by base stacking and to a lesser degree by base pairing interactions.[2−4] A technique called "bulge hybridization" has been used to track annealing processes between 3-MI-containing strands and complements. In this method, the 3-MI molecule is treated as an insertion and does not have a base-pairing partner in the complement. As the two strands come together, the 3-MI may be pushed out of the base stacking interaction, thereby releasing quench. Up to 20-fold increases in fluorescence intensity have been observed in this sequence-dependent method.[4] 3-MI is commercially available and can be purchased incorporated into custom oligonucleotides from TriLink Biotechnologies, Inc., San Diego, CA or in phosphor-amidite form from Toronto Research Chemicals, (TRC) Toronto, Canada.

The benefit of 3-MI's high quantum yield is offset by the disadvantage of the small absorption cross section with a maximum in the near UV. We measure the extinction coefficient of 3-MI in buffer to be 13 000 ± 100 L/mol·cm at 351 nm. For comparison, the extinction coefficient of Cy3, a popular DNA label used in single-molecule fluorescence studies, is 150 000 L/mol·cm at its absorption maximum with a quantum yield of fluorescence = 0.1 (although this value is strongly dependent on the rigidity of the local environment and can be much larger[9]); in the absence of photobleaching or saturation, the fluorescence intensity from 3-MI should be only slightly smaller than Cy3 under comparable excitation conditions. On the other hand, the extinction coefficient of 2-AP is only 5400 L/mol·cm at its absorption maximum,[7] with a quantum yield of 0.66.[10] A major challenge for single-molecule detection using UV fluorescence microscopy is presented by very high background fluorescence in the UV range. The photoluminescence of optics and substrates in the UV, particularly that originating from the coverslip, immersion oil, and the objective lens, is a major source of background fluorescence. The second source is Raman scattering from the 3400 cm^{-1} O−H stretching mode of water, which has a cross section that is 5 times larger at 350 nm than at 475 nm.[11]

We present results demonstrating single-molecule sensitivity for one-photon fluorescence detection of 3-MI with a signal-to-background ratio above 5 and a quantum yield of photobleaching = 2.5×10^{-3}. We use fluorescence correlation spectroscopy (FCS)[12−14] following the analysis used in refs 15 and 16 to determine absolute values for the fluorescence count rate per molecule (η) and the fluorescence signal-to-background ratio per molecule (S/B) as a function of excitation intensity, and to estimate the photobleaching rate (k_b). Our time resolution is not adequate to determine the intersystem crossing (k_{ISC}) and triplet decay rates (k_T) for 3-MI, but we can determine an upper limit to the ratio k_{ISC}/k_T. We also model the saturation of η using k_b and k_{ISC}/k_T[8,17] and compare the results to our measurements. Results for η and S/B are presented for the 3-MI monomer, a 3-MI-containing single-strand, and a laser dye molecule with a similar fluorescence spectrum, stilbene 3.

2. Materials and Methods

2.1. Samples. Measurements were performed on three molecules: 3-MI, a single-stranded DNA incorporated with 3-MI (36-mer), and, for comparison, a laser dye molecule, stilbene 3. We prepared a 160 μM stock solution of 3-MI by dissolving solid 3-MI in water (all water used is UV-treated, filtered, and deionized water at 18 MΩ), ultrasonicating and heating the solution at approximately 45 °C for 15 min, and then filtering the room-temperature solution using a 0.2 μm syringe filter. This stock solution was diluted with water to 1.6 nM for the FCS measurements. The 36-mer had the following sequence: 5′-**F**tc ctg gga tta aat aaa ata gta aga atg tat agc-3′, where **F** denotes the 3-MI. A 3.1 μM solution of the 36-mer in 10 mM Tris-Cl pH 7.5 was diluted with water to 2.0 nM. Stilbene 3 was dissolved and diluted in water to 1.0 nM. Fluorescence from a water sample was measured to determine the background contribution to the fluorescence intensity. FCS was performed on the same water sample to confirm that there were no measurable fluorescent impurities. For FCS measurements, the solutions were held in a 150 μL well made of poly-(dimethylsiloxane) (PDMS, Sylgard 184) on a glass coverslip (Fisher Premium #1). Before attachment of the PDMS well, the glass coverslip was cleaned for 30 min in a UV-ozone cleaner, which substantially reduces background fluorescence at the surface.

2.2. Fluorescence Correlation Spectroscopy Measurements. The FCS measurements were performed on a home-built inverted confocal fluorescence microscope. An argon ion laser was used to provide 351.1 nm continuous wave excitation, selected (instead of the stronger 363.8 nm line) because it is closest to the 3-MI absorption maximum and places water's O−H stretch Raman line at 400 nm, which is 30 nm shorter than 3-MI's emission maximum. The laser intensity was controlled with a half-wave plate followed by a polarizing cube. A BK7 prism allowed spectral selection of the 351.1 nm line from other wavelengths emitted from the argon ion tube. The laser beam was spatially filtered and expanded using a telescope and a 50 μm pinhole. A second telescope was used to adjust the diameter and convergence of the laser beam entering the objective. The diameter of the laser beam entering the objective was roughly one-half the back-focal plane aperture diameter, so that the back aperture was under-filled, as required to minimize artifacts in the FCS analysis.[18] A dichroic filter (Omega 400DCLP) directed the laser beam into an inverted oil immersion objective lens (Zeiss Fluar, 1.3 NA, 100×, $f = 1.65$ mm, infinity-corrected). A silicon photo-diode measured the 351.1 nm excitation that was transmitted through the dichroic filter. Prior measurement of the dichroic's transmission (2%) allowed conversion of the photodiode power to power entering the objective lens. The objective lens transmitted roughly 70% of the incident excitation. The excitation intensities used in this report were calculated using this power measurement and the radius of the focused spot. The radius of the focused spot was determined from FCS measurements to be 0.31 μm.

The coverslip with PDMS well was placed above the objective. The focus was monitored by imaging the back-reflected laser beam (reflected from the glass/solution interface) onto a CCD video camera. The fluorescence was collected using the same objective lens. The dichroic filter and a band-pass filter (Chroma HQ450/ 80M) block the 351.1 nm excitation and the 400 nm water Raman line. A 100 mm focal length achromatic doublet lens focused the fluorescence through a 50 μm diameter
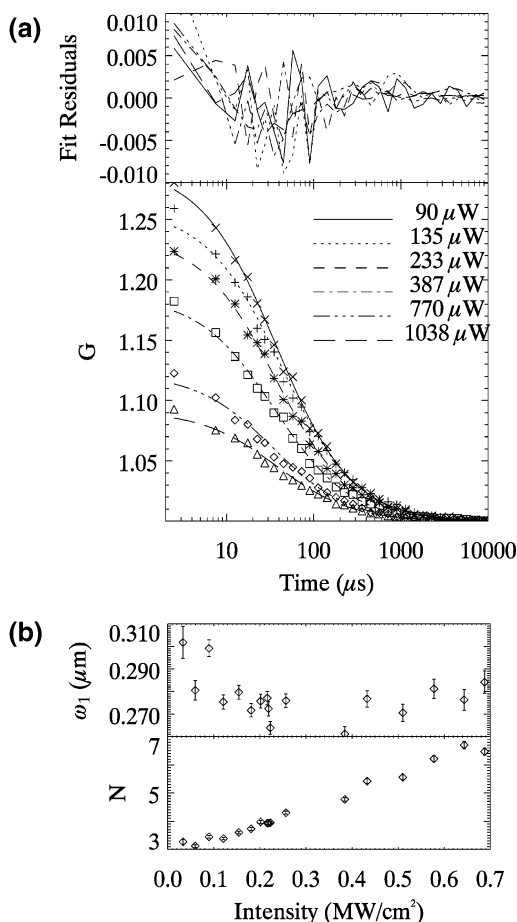
(a)

(b)

Figure 2. (a) Bottom: Measured autocorrelation function for 3-MI monomer in water at various excitation power levels (symbols) and corresponding fit to the data using eq 2 (lines). Top: Fit residuals. The time axis has been shifted 2.5 μs to accommodate plotting the point at $t = 0$. (b) Fit parameters as a function of excitation intensity.

(a)

(b)

Figure 3. (a) Bottom: Measured autocorrelation function for stilbene 3 in water at various excitation power levels (symbols) and corresponding fit to the data using eq 2 (lines). Top: Fit residuals. The time axis has been shifted 2.5 μs to accommodate plotting the point at $t = 0$. (b) Fit parameters as a function of excitation intensity.

confocal pinhole (approximately a factor of 2 greater than the optimal diameter discussed in ref 18). Behind the pinhole was a Hamamatsu H7421-40 GaAsP photomultiplier photon-counting detector with approximately 25% QE at 425 nm and a dark count rate below 10 per second. A PC equipped with a data acquisition board and LabView software counted photon pulses from the detector. The PC also controlled an electromechanical shutter that blocked the excitation for periods between measurements.

For FCS measurement, the PDMS well was filled with solution. The excitation light was focused onto the glass/solution interface; the focus was then translated 50 μm into the solution to reduce background from the coverslip and immersion oil by 85%. Fluorescence intensity (photon count rate) was measured as a function of time with 5 μs resolution. Ten consecutive runs lasting 10 s were recorded, giving a total measurement time of 100 s. Measurements were taken at input power levels (power into the objective lens) between 10 μW and 1.1 mW. After a solution was measured, the PDMS well and coverslip were rinsed with pure water and reused.

The normalized fluorescence intensity autocorrelation function, $G(\tau)$, is defined by

$$G(\tau) = \frac{\langle I(t)I(t+\tau)\rangle}{\langle I(t)\rangle^2} \qquad (1)$$

where $I(t)$ is the measured intensity in counts as a function of time and the brackets denote a temporal average. Autocorrelation
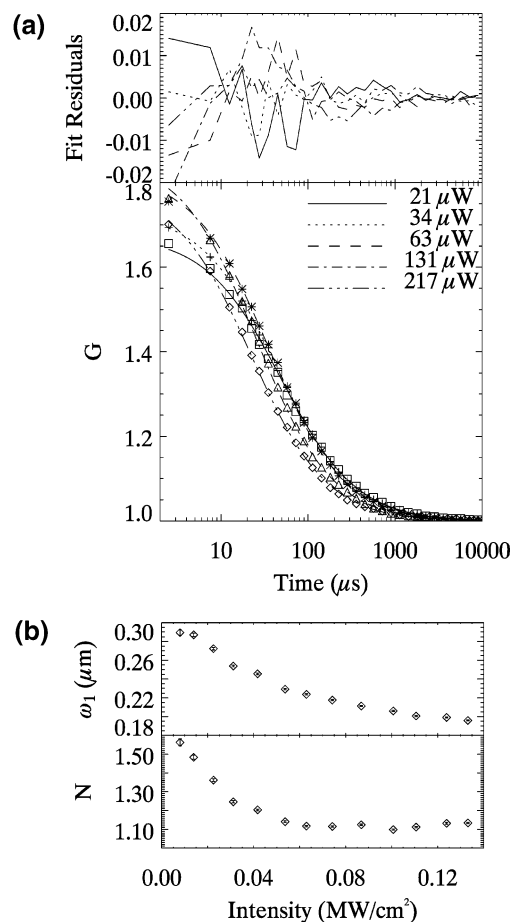
on the last 5 s of each 10 s data set was performed using a software-implemented fast Fourier transform method. The autocorrelations for the 10 runs were then averaged. Typical autocorrelation functions are shown in Figures 2−7.

2.3. Fluorescence Correlation Spectroscopy Analysis. In FCS, the temporal fluctuations in fluorescence intensity that occur as a result of diffusion through a focal volume and molecular photophysics, photochemistry, or chemistry are analyzed to obtain parameters such as the diffusivity of the fluorescing species; the number of fluorescent molecules in the focal volume, N, and the intensity (count rate) per molecule (η); the photobleaching rate constant (k_b); and the triplet correlation time (t_T) and triplet fraction (T), or alternately the intersystem crossing rate (k_{ISC}) and triplet lifetime (k_T).[15,16,19−21]

For a simple two-state system in the absence of photobleaching, an analytical expression for the normalized autocorrelation function, $G_D(\tau)$, is obtained by approximating the product of the excitation intensity and the collection efficiency profiles, $W(r)$, as a three-dimensional Gaussian: [21−23]

$$G_D(\tau) = 1 + \frac{(1 - \langle I_B(t)\rangle/\langle I(t)\rangle)^2}{N}\left(1 + \frac{4D\tau}{\omega_1^2}\right)^{-1}\left(1 + \frac{4D\tau}{\omega_2^2}\right)^{-1/2} \qquad (2)$$

where I_B is the background contribution to the fluorescence intensity,[20,24] I is the total fluorescence intensity, N is the average
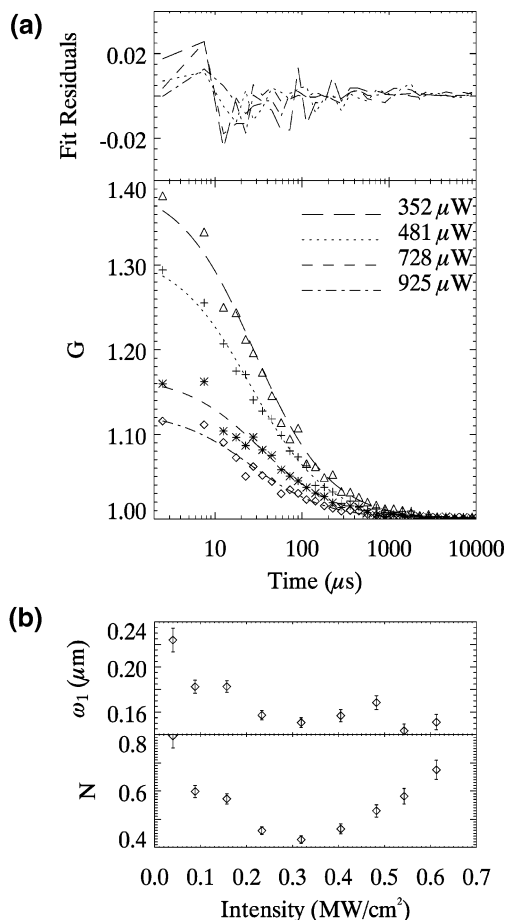
(a)

(b)

Figure 4. (a) Bottom: Measured autocorrelation function for the 36-mer in water at various excitation power levels (symbols) and corresponding fit to the data using eq 2 (lines). Top: Fit residuals. The time axis has been shifted 2.5 μs to accommodate plotting the point at $t = 0$. (b) Fit parameters as a function of excitation intensity.

number of molecules in the observation volume, D is the diffusion constant, ω_1 is the $1/e^2$ distance of $W(\mathbf{r})$ in the radial direction (in the $x-y$ plane), and ω_2 is the $1/e^2$ distance of $W(\mathbf{r})$ in the axial direction (z). The background contribution I_B originates mainly from UV-induced photoluminescence of optics in the confocal fluorescence microscope (e.g., the glass coverslip, the immersion oil, and the objective lens). Here, we estimate values for the diffusion constant D using the Stokes–Einstein equation, $D = kT/6\pi\eta_w r$, where k is the Boltzmann constant, $T = 298$ K, η_w is the viscosity of water (0.01 g cm^{-1} s^{-1}), and r is the hydrodynamic radius of the molecule. The hydrodynamic radius is estimated by assuming a spherical molecule with known molecular mass M and density ρ, as $r = \sqrt[3]{3M/4\pi\rho N_A}$. The diffusion constant estimates for the three species investigated in this study are: 3-MI, $D = 5 \times 10^{-6}$ cm^2/s; stilbene 3, $D = 4 \times 10^{-6}$ cm^2/s; and 36-mer DNA, $D = 2 \times 10^{-6}$ cm^2/s.

Photochemical reactions (photobleaching) and photophysics (triplet state dynamics and saturation) will modify the autocorrelation function. Photobleaching can occur while the molecule diffuses across the observation volume, causing an apparent decrease in ω_1 and ω_2 as the excitation intensity P increases. Because N is determined by $G_D(0)$, the value of N is for the most part unaffected by photobleaching. On the other hand, where singlet–triplet transitions occur on a much shorter timescale than the diffusion time,[25] the population of a triplet state
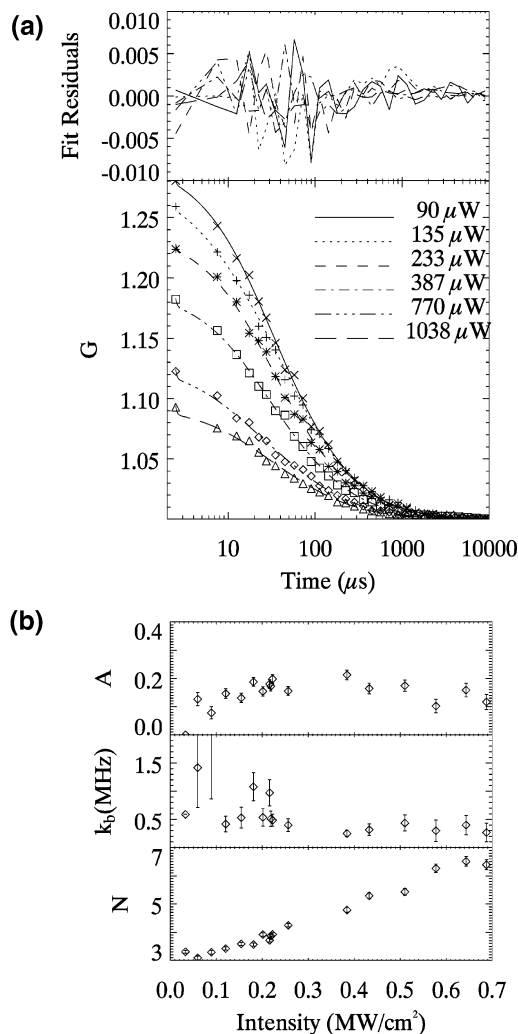
(a)

(b)

Figure 5. (a) Bottom: Measured autocorrelation function for 3-MI monomer in water at various excitation power levels (symbols) and corresponding fit to the data using eq 3 (lines). Top: Fit residuals. The time axis has been shifted 2.5 μs to accommodate plotting the point at $t = 0$. (b) Fit parameters as a function of excitation intensity. The values for k_b and A at the lowest three intensity levels are meaningless due to the insensitivity of the fits to photobleaching at these intensities, but for completeness, the value for k_b at 0.09 MW/cm^2 (which is not shown in the plot) is 3.2 MHz $\pm$ 2.4 MHz.

can reduce the apparent value for N with increasing P, and might also reduce the apparent value of ω_1 and ω_2. When triplet and photobleaching dynamics are included, the autocorrelation function for a three-level system (ground state, excited state, triplet state) has been approximated as:[15,25,26]

$$G(\tau) = 1 + \frac{(G_D(\tau) - 1)}{(1 - T)}[1 - A(1 - T) + A(1 - T)\exp(-k_{bl}\tau) - T + T\exp(-\tau/t_T)] \quad (3)$$

where T is the equilibrium fraction of molecules in the triplet state, t_T is the triplet correlation time, and k_{bl} is the average effective photobleaching rate of a fraction A of excited molecules. In this approximation, the effective photobleaching rate, which depends on the intensity, is taken to be a constant across a portion of the beam profile, and zero elsewhere.[15] The triplet correlation time t_T depends on several rate constants that describe a three energy level system:[26] the triplet decay rate constant, k_T; the intersystem crossing rate constant from the
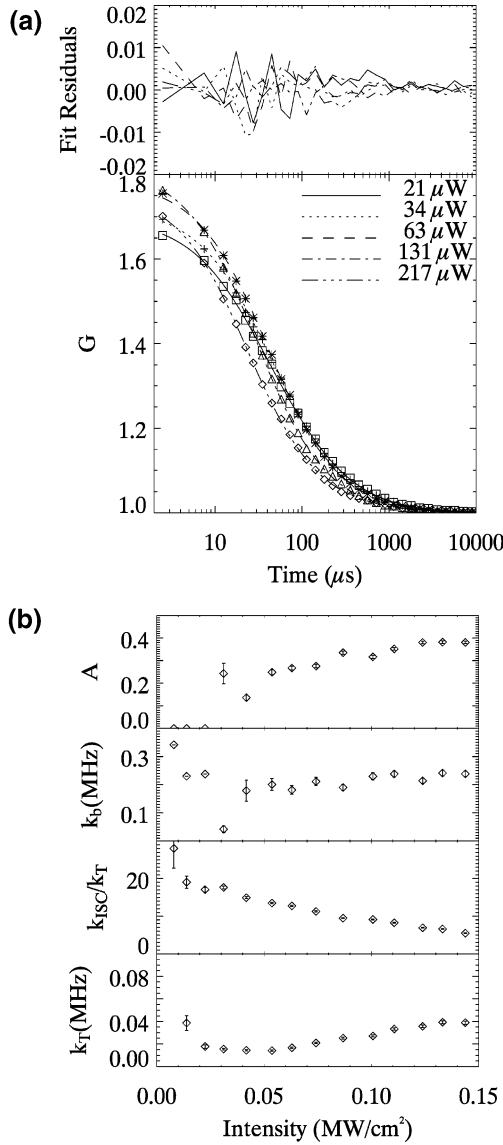
(a)

(b)

Figure 6. (a) Bottom: Measured autocorrelation function for stilbene 3 in water at various excitation power levels (symbols) and corresponding fit to the data using eq 3 (lines). Top: Fit residuals. The time axis has been shifted 2.5 μs to accommodate plotting the point at $t = 0$. (b) Fit parameters as a function of excitation intensity.

excited singlet state to the triplet state, k_{ISC}; the radiative decay rate, k_f; the nonradiative (internal conversion) rate k_{IC}; and the excitation rate, $\sigma P / h\nu$, where σ is the absorption cross section at 351 nm. For $(\sigma P / h\nu + k_{IC} + k_f) \gg (k_{ISC} + k_T)$:[26]

$$\frac{1}{t_T} = \left(k_T + \frac{\sigma P}{h\nu} \cdot \frac{k_{ISC}}{\frac{\sigma P}{h\nu} + k_{IC} + k_f} \right) \qquad (4)$$

We define

$$k_0 \equiv 1/\tau_f = k_f + k_{IC} + k_{ISC} \qquad (5)$$

where τ_f is the fluorescence lifetime. The triplet fraction, T, is then given by:[26]

$$T = \frac{\sigma P}{h\nu} \cdot \frac{k_{ISC}}{\frac{\sigma P}{h\nu}(k_{ISC} + k_T) + k_0 k_T} \qquad (6)$$
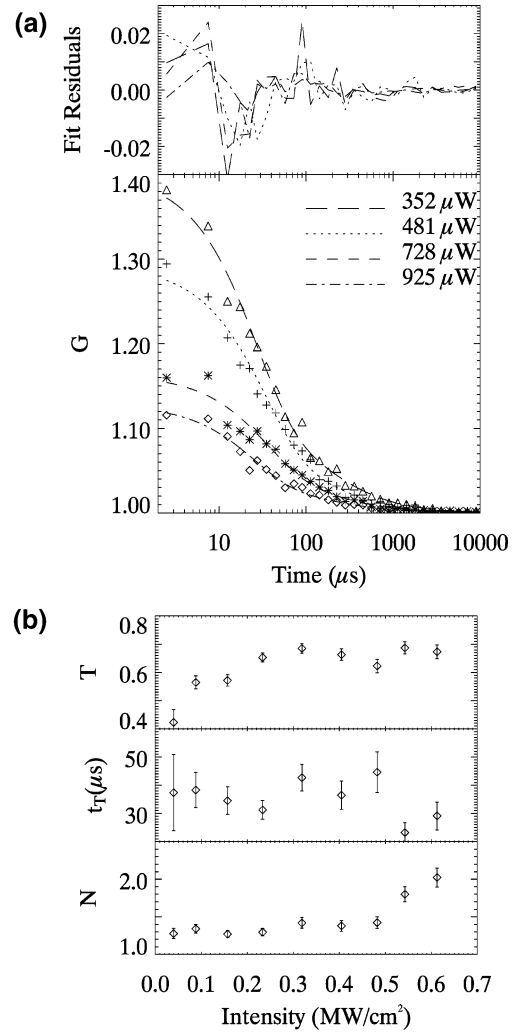
(a)

(b)

Figure 7. (a) Bottom: Measured autocorrelation function for the 36-mer in water at various excitation power levels (symbols) and corresponding fit to the data using eq 3 (lines). Top: Fit residuals. The time axis has been shifted 2.5 μs to accommodate plotting the point at $t = 0$. (b) Fit parameters as a function of excitation intensity.

The effective photobleaching rate, which is a function of the excitation intensity, is given in terms of the power-independent microscopic rates as

$$k_{bl} = \left(\frac{\sigma P}{h\nu} \frac{k_b k_T}{\frac{\sigma P}{h\nu}(k_{ISC} + k_T) + k_0 k_T} \right) \qquad (7)$$

where $k_b = k_{bS} + k_{bT} k_{ISC}/k_T$ and k_{bT} and k_{bS} are the bleaching rates out of the triplet and single states, respectively. Note this is the form of k_{bl} derived in ref 15 for a three-level system. In this case, k_{bl} increases with excitation intensity P and saturates at high P.

One important effect that is not included in either approximation (eqs 2 and 3) is the depletion of the ground state (saturation of the singlet−singlet transition) that occurs with increasing P. Depletion will lead to broadening of the spatial fluorescence profile, an effective increase in the detection volume, which in turn will lead to an increase of N.[25] Values for ω_1 and ω_2 will increase with $N^{1/3}$.

2.4. Fluorescence Intensity Saturation Measurements and Analysis. Using FCS measurements and analysis, we determined the number of photons per molecule emitted as a function of power. In terms of the rates defined above, the steady-state

average fluorescence count rate as a function of power is expected to follow a saturation curve represented by

$$\bar{I} = \alpha \frac{k_f}{k_0} \frac{\sigma}{h\nu} P \left(\frac{1}{1 + P/P_s} \right) \left(\frac{1}{1 + P/P_b} \right) \quad (8)$$

where I is measured in photons/second, and α is a constant proportional to the concentration of the solution and the light collection efficiency of the microscope. The first term in parentheses reflects the effect of ground-state depletion (saturation of the singlet−singlet transition). The saturation intensity P_s is given by

$$P_s = \left[\frac{1}{k_0} \frac{\sigma}{h\nu} \left(1 + \frac{k_{ISC}}{k_T} \right) \right]^{-1} \quad (9)$$

The second term in parentheses in eq 8 reflects the effect of photobleaching:[8,17]

$$P_b = \left[\frac{k_b}{k_0} \frac{\sigma}{h\nu} \tau_D \right]^{-1} \quad (10)$$

where k_b is the bleaching rate constant and τ_D is the time a freely diffusing molecule spends in the observation volume. We assume that $\tau_D = \omega_1^2/4D$.

3. Results and Discussion

Autocorrelation functions were obtained for the three samples described above, for laser excitation powers between 10 μW and 1.1 mW. Fits of eq 2 or eq 3 to the data were performed using a Levenberg−Marquardt least-squares algorithm; uncertainties corresponding to ± 1 standard deviation of the fitting parameter are reported along with the fitting parameter in all cases.

Figure 2a displays data for $G(\tau)$ of 3-MI monomer taken at various power levels. Fits of eq 2 to the data are shown as lines, and the residuals (data-fit) are plotted above the data. The only adjustable parameters in the fit shown in Figures 2−4 are N and ω_1. The axial width of $W(\mathbf{r})$, ω_2 in eq 2, is taken to be 7 times ω_1; the fits are relatively insensitive to this parameter, and a factor of 7 is a reasonable estimate for our geometry. The parameters N and ω_1 are shown in Figure 2b as a function of the intensity at the center of the focal volume. The intensity at the center of the focal volume is calculated using the measured excitation power and the value for the radius of the focused spot that is determined from fits to the autocorrelation function at low powers (from eight separate data sets all taken at input power between 8 and 80 μW, not shown, the radius at low power is 0.311 $\pm$ 0.002 μm).

Systematic deviation of the fit from the data at times less than 100 μs in Figure 2a is consistent with neglecting triplet and/or photobleaching dynamics. An inspection of the best-fit values for N and ω_1 in Figure 2b indicates the following. First, the obvious marked increase in N with power is consistent with ground-state depletion (singlet saturation)[25] as discussed above. The increase in ω_1 commensurate with this increase in N is small and masked by an apparent decrease in the focal volume at low powers, but is evident at high power. The decrease in the focal radius for the lowest power measurements shown in Figure 2b is most likely indicative that photobleaching dominates the behavior of ω_1 in this regime. For 3-MI, P_b is an order of magnitude less than P_s (see below); changes in fit parameters with power that are due to photobleaching will therefore be more apparent for the low power points in Figure 2b, where effects

due to ground-state depletion are minor. Note at even lower power (not shown) ω_1 goes to a constant 0.31 μm, as discussed above. From eqs 3 and 6, we see that the effect of a triplet would be an apparent decrease in N with power (increase $G(0)$), and so from this initial fit we see no evidence of a triplet in the 3-MI monomer. As we show below, our 5 μs sample time does not permit resolution of 3-MI's triplet lifetime, but our measurements do allow us to put an upper limit on the small triplet fraction for 3-MI monomer.

For comparison, we show in Figure 3a the corresponding data and fit for stilbene 3. Again, systematic deviations from the form given in eq 2 are visible at short times, but here the best-fit values of N and ω_1 (Figure 3b) show clear evidence of both triplet and photobleaching dynamics. The decrease in ω_1 with power is consistent with photobleaching, while the decrease in N with power is a clear indication that a triplet population is present (eqs 2 and 3). Ground-state depletion is only weakly evident for stilbene 3 as a flattening of the ω_1 curve and the very slight increase in N at high power.

When 3-MI is incorporated into DNA, sequence-dependent quenching can result.[2−4] In Figure 4, we show $G(\tau)$ data and fits of eq 2 for the 36-mer described in the Materials and Methods section. Here, we see deviations from a good fit similar to those seen in the 3-MI monomer; however, the best-fit parameters (Figure 4b) tell a somewhat different story. Here, the initial decrease in both N and ω_1 indicates that photobleaching and the triplet population are growing with excitation power, similar to the case for stilbene 3. The marked increase in N at high power also shows the effects of ground-state depletion similar to 3-MI monomer.

In Figures 5−7, we fit eq 3 to the data in an attempt to improve the goodness of fit and determine the photophysical properties of the various fluorophores. There are at most seven parameters that could be fit to the data. For example, given the diffusivities of the molecules we are studying, we could in principle fit k_{bl}, A, T, t_T, N, ω_1, and ω_2 to the data. Alternately, if values for τ_f and σ are known, we can use eqs 4−7 to replace the effective parameters k_{bl}, T, and t_t with the power-independent microscopic parameters k_b, k_{ISC}, and k_T; the choice of fit parameters $R = k_{ISC}/k_T$, k_T, and k_b gives a more satisfactory fit (the parameters are less correlated). The values for absorption cross section and fluorescence lifetime for 3-MI monomer and for stilbene 3 are given in Table 1. We can reduce the number of parameters by one by recalling that the fits are relatively insensitive to ω_2 and so set $\omega_2 = 7 \times \omega_1$, as is reasonable for our geometry. In general, without a faster time resolution and higher signal-to-noise ratio than are available here, it is not possible to fit all six remaining parameters, although we can use the fits shown in Figures 2−4, as well as the correlation matrixes from the fits, to guide our choice of fixed and fitted parameters.

In the case of 3-MI monomer, we recall that there was no obvious triplet evident from the fit to eq 2. We nonetheless attempt fits for $R = k_{ISC}/k_T$, k_T, k_b, N, and A, holding ω_1 constant and again using $\omega_2 = 7 \times \omega_1$. The results are completely insensitive to the value of k_T, as might be expected from our 5 μs time resolution. The uncertainty in R is also large from these fits, but here we can define a clear upper limit; $R < 0.5$. Values of $R \geq 0.5$ result in clear increases in the value of χ^2 for all fits; for smaller values of R, the χ^2 are all very close to 1 with no systematic deviations. Note also that $R < 0.5$ also implies an upper limit, at high power (such that $\sigma P/h\nu \gg k_0$), on the triplet fraction of $T < 0.3$ (eq 6). We choose an intermediate value, $R = 0.3$, fix $k_T = 10$ MHz, and perform fits to find A,

TABLE 1: Photophysical Parameters for Stilbene 3 and 3-MI (Uncertainties (1 standard deviation) Are Given in Parentheses Where Appropriate; σ and ϵ Are Measured at 351 nm)

	τ_ϕ (ns)	σ (cm^2)	ϵ (L/mol·cm)	k_b (kHz)	k_{ISC}/k_T	P_s (MW/cm^2)	P_b (MW/cm^2)
3-MI	6.5[a]	4.98×10^{-17}	13 000 (100)	389 (30)	<0.5	1.3	0.094
stilbene 3	1.2[b]	2.54×10^{-16}	66 500 (700)	203 (4)	5−20		0.15

[a] See ref 27. [b] Knutson, J. R.; Smirnov, A. V. National Heart, Lung, and Blood Institute, personal communication, 2003.

k_b, and N. The results of these fits are shown in Figure 5. Note that the obvious systematic deviations are gone from the residuals. The parameter A does not change significantly with power, as expected. The bleaching rate constant k_b also shows no obvious trend with power and has a weighted average value of $k_b = 389 \pm 20$ kHz. If we use this value for the bleaching rate, we can calculate the quantum yield of photobleaching, $\phi_b = k_b \cdot \tau_f = 2.5 \times 10^{-3}$, from which we can predict approximately 395 cycles before 3-MI photobleaches in this aqueous environment.

For stilbene 3, which has a higher cross section and is considerably brighter than 3-MI, it is possible to fit more parameters directly. We fix ω_1 and ω_2 as before, and, because the effects of ground-state depletion are minimal in this sample, we fix $N = 1.65$. This value was chosen because it gave the lowest values for χ^2 and is consistent with the lower power data shown in Figure 3b. We then fit the remaining parameters, k_b, R, k_T, and A; results are shown in Figure 6. The χ^2 for these fits is again close to 1 in all cases. Ignoring the three lowest intensity data points, for which the fits need not include triplet or bleaching effects to be good fits, we find the following. First, the value for A is somewhat higher for stilbene 3 than for 3-MI, and it seems to show a weak trend with power that we do not understand. The bleaching rate k_b is a constant value $\cong 0.2$ MHz (see Table 1) where it is measurable, which is an indication that our use of a three-level model for photobleaching is reasonable. However, there is strong trend in R with power and an equally strong trend in k_T. Interestingly, multiplying k_T by R gives a constant $k_{ISC} = 0.241 \pm 0.002$ MHz. The behavior of k_T, R, and k_{ISC} is not consistent with a three-level system but might be explained, for example, if the molecule was excited out of the long-lived triplet state into a shorter-lived higher-energy triplet state at high excitation intensity. The triplet fraction in stilbene 3 (calculated from eq 6) is significant and goes to a constant of approximately 0.33 at the highest powers measured. Extrapolation of T to the high power limit (such that $\sigma P/h\nu \gg k_0$) is impossible because of the trend in R. The quantum yield of photobleaching for stilbene 3 is $\phi_b = k_b \cdot \tau_f = 2.4 \times 10^{-4}$.

In Figure 7, we show the results of a fit to the autocorrelation function for the 36-mer described above. Here, we have once again fixed ω_1 and ω_2, and we have also set the bleaching parameter A to zero; we ignore bleaching in this fit. The signal-to-noise ratio is not adequate to permit a fit of the bleaching and triplet parameters, and k_{bl} and t_T tend to be correlated in the fits. The χ^2 of these fits is close to 1, but without including bleaching parameters there are obvious deviations from a good fit evident in the residuals. It is not at all clear that this triplet fit is an improvement over the diffusion fit shown in Figure 4, and this is probably because bleaching effects do come into play, as discussed above. Nonetheless, we note that the triplet fit correctly results in a constant N at low powers and the upturn in N at higher powers is again indicative of ground-state depletion. The value $N \cong 1.3$ is direct evidence that single 3-MI containing oligonucleotides are detectable. The saturation value for the triplet fraction, T (Figure 7b), is quite robust (the same
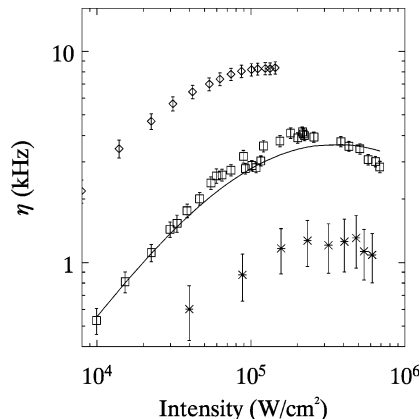

Figure 8. The count rate per molecule, η, is plotted as a function of the input intensity. $\diamond$: stilbene 3. $\square$: 3-MI monomer. *: 36-mer. Line: eq 8 plotted using values for P_s and P_b determined from the fit shown in Figure 5b.

value results even when including bleaching parameters in the fit), and so we can conclude that, unlike the monomer, there is a very significant triplet population $T \cong 0.7$ in the incorporated analogue. We note that, while it seems to us most likely that the triplet population of 3-MI is what we are measuring here, we cannot distinguish in these measurements between triplet and other dark states of the oligo-incorporated molecule. The correspondingly larger triplet (or dark) fraction is consistent with the decrease in brightness of this sample as compared to the monomer.

Using the fits shown in Figures 5−7, we can calculate values for the number of photons per molecule emitted as a function of power, denoted η and shown in Figure 8. This figure also includes data for 3-MI taken at lower powers than shown in Figure 5; the lower power data have been scaled down slightly to accommodate different instrument sensitivities on the 2 days that data were taken (the ratio of sensitivities was 0.74). The error bars in Figure 8 (± 1 standard deviation) are from a propagation of uncertainties in I, I_B, and the uncertainty in the fit for N. For 3-MI monomer, the fits shown in Figure 5b and discussed in the text allow us to calculate the bleaching saturation power, P_b, from eq 10 and the singlet saturation power, P_s, from eq 9. With $R = 0.3$, we find $P_b = 94$ kW/cm^2 and $P_s = 1.3$ MW/cm^2. Using eq 8, these two values permit us to calculate η, except for a prefactor that depends in part on instrument sensitivity. We perform a single parameter fit to the 4 lowest power data points to account for the prefactor. The fit, with a prefactor of 0.0618 ± 0.0007 kHz/(W/cm^2) is shown as a solid line in Figure 8. There is an obvious discrepancy, but the maximum value for η is only slightly lower for the model.

In Figure 9, we divide η by the background signal at each power level and plot the signal/background (S/B) ratio per molecule. These parameters along with the quantum yield of photobleaching determine how well a molecule will perform in a single-molecule experiment.
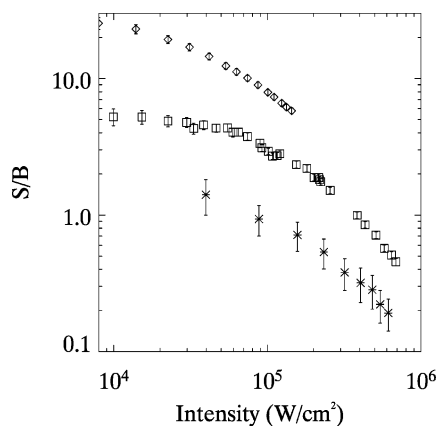
Figure 9. The signal-to-background ratio (*S/B*) for each sample is shown. ◇: stilbene 3. □: 3-MI monomer. *: 36-mer.

4. Conclusions

For 3-MI to be useful in single-molecule detection, it must be sufficiently bright to overcome background, and stable against photobleaching. As compared to chromophores excited at visible wavelengths, it would seem a weak candidate. Yet as compared to other nucleic acid analogues, most of which are excited in the UV, 3-MI seems promising.

We see in Figures 8 and 9 that 3-MI monomer has a maximum $\eta = 4$ kHz and a single-molecule signal-to-background ratio of approximately 5. This compares quite favorably to 2-AP, which has a maximum $\eta = 2$ kHz but thus far an *S/B* of only 0.3.[7] Coumarin-120 (excitation at 350 nm), while not itself an analogue, has been proposed as a candidate for single-molecule DNA measurements.[20] Brand et al. report on FCS data taken specifically to investigate photobleaching of coumarin-120. In this case, they expand the focal volume to better measure bleaching constants, which unfortunately also increases the background. They report a total count rate of 24 kHz and a background rate of 9.4 kHz for a total of 14.6 kHz coming from 61 molecules in the beam, for an average count rate per molecule of 240 Hz, more than an order of magnitude lower than 3-MI. [However, Brand and others (1997) report a *S/B* for single photon excitation of coumarin-120 as high as 400. We note that this number is measured using a substantially different technique than that used here and does not represent an average value. With a very low probability of more than one molecule in the detection volume, Brand et al. observe the fluorescence counts in 1 ms bins versus time directly and observe spikes in the count rate as high as 13 000 at a background level of 380 Hz. They divide 13 000 by the diffusion time measured by FCS and thereby obtain values for *S/B* as high as 400.] For two-photon excitation (TPE), coumarin improves substantially. Brand et al. measure an average TPE count rate per molecule of 25 kHz and a *S/B* of 52 (from Figure 4 in ref 20).

As we see for tryptophan,[8] photostability is problematic for many if not most UV chromophores. For the coumarins,[15] the k_b's reported at low excitation power are as much as an order of magnitude lower than the bleaching rate found here for 3-MI monomer. However, it can be difficult to compare measurements taken at low power to those measured at higher power, where a three-level approximation might break down.

There is clear room for improvement of both photobleaching rates and signal-to-background ratios for 3-MI. If the case of coumarin-120 is not unique, then both photostability and *S/B* might be substantially improved by the use of two-photon excitation.[15,20] The use of oxygen scavengers might also substantially decrease the quantum yield of photobleaching. It is not unreasonable to expect that replacement of our relatively inexpensive objective lens and ordinary glass coverslips with higher quality optics might result in an order of magnitude reduction of background.

In summary, we have demonstrated single-molecule sensitivity for the detection of 3-MI monomer with a signal-to-background ratio as high as 5 and a count rate per molecule above 4 kHz. We have shown that when 3-MI is incorporated into a strand of DNA, the triplet fraction substantially increases. This is consistent with the well-documented and sequence-dependent quenching of 3-MI's fluorescence when incorporated into DNA.[2-4] Despite the decrease in brightness, we have shown that 3-MI-containing oligonucleotide is also detectable on a single-molecule basis with a signal-to-background ratio greater than 1.

References and Notes

(1) Rist, M. J.; Marino, J. P. *Curr. Org. Chem.* **2002**, *6*, 775.
(2) Hawkins, M. E.; Pfleiderer, W.; Mazumder, A.; Pommier, Y. G.; Falls, F. M. *Nucleic Acids Res.* **1995**, *23*, 2872.
(3) Driscoll, S. L.; Hawkins, M. E.; Balis, F. M.; Pfleiderer, W.; Laws, W. R. *Biophys. J.* **1997**, *73*, 3277.
(4) Hawkins, M. E. *Cell Biochem. Biophys.* **2001**, *34*, 257.
(5) Deprez, E.; Tauc, P.; Leh, H.; Mouscadet, J. F.; Auclair, C.; Hawkins, M. E.; Brochon, J. C. *Proc. Natl. Acad. Sci. U.S.A.* **2001**, *98*, 10090.
(6) Hill, J. J.; Royer, C. A. Fluorescence Approaches to Study of Protein-Nucleic Acid Complexation. In *Methods in Enzymology—Fluorescence Spectroscopy*; Brand, L., Johnson, M. L., Eds.; Academic Press: New York, 1997; Vol. 278.
(7) Wennmalm, S.; Blom, H.; Wallerman, L.; Rigler, R. *Biol. Chem.* **2001**, *382*, 393.
(8) Lippitz, M.; Erker, W.; Decker, H.; Van Holde, K. E.; Basche, T. *Proc. Natl. Acad. Sci. U.S.A.* **2002**, *99*, 2772.
(9) Mujumdar, R. B.; Ernst, L. A.; Mujumdar, S. R.; Lewis, C. J.; Waggoner, A. S. *Bioconjugate Chem.* **1993**, *4*, 105.
(10) Holmen, A.; Norden, B.; Albinsson, B. *J. Am. Chem. Soc.* **1997**, *119*, 3114.
(11) Faris, G. W.; Copeland, R. A. *Appl. Opt.* **1997**, *36*, 2686.
(12) Magde, D.; Elson, E. L.; Webb, W. W. *Phys. Rev. Lett.* **1972**, *29*, 705.
(13) Magde, D.; Elson, E. L.; Webb, W. W. *Biopolymers* **1974**, *13*, 29.
(14) Elson, E. L.; Magde, D. *Biopolymers* **1974**, *13*, 1.
(15) Eggeling, C.; Widengren, J.; Rigler, R.; Seidel, C. A. M. *Anal. Chem.* **1998**, *70*, 2651.
(16) Dittrich, P. S.; Schwille, P. *Appl. Phys. B* **2001**, *73*, 829.
(17) Mertz, J. *Eur. Phys. J. D* **1998**, *3*, 53.
(18) Hess, S. T.; Webb, W. W. *Biophys. J.* **2002**, *83*, 2300.
(19) *Single Molecule Detection in Solution, Methods and Applications*; Zander, C., Enderlein, J., Keller, R. A., Eds.; Wiley-VCH: Berlin, 2002.
(20) Brand, L.; Eggeling, C.; Zander, C.; Drexhage, K. H.; Seidel, C. A. M. *J. Phys. Chem. A* **1997**, *101*, 4313.
(21) Thompson, N. L. Fluorescence Correlation Spectroscopy. In *Topics in Fluorescence Spectroscopy*; Lakowicz, J. R., Ed.; Plenum Press: New York, 1991; Vol. 1, p 337.
(22) Qian, H.; Elson, E. L. *Appl. Opt.* **1991**, *30*, 1185.
(23) Rigler, R.; Mets, U.; Widengren, J.; Kask, P. *Eur. Biophys. J. Biophys. Lett.* **1993**, *22*, 169.
(24) Koppel, D. E. *Phys. Rev. A* **1974**, *10*, 1938.
(25) Widengren, J.; Mets, U.; Rigler, R. *J. Phys. Chem.* **1995**, *99*, 13368.
(26) Widengren, J.; Rigler, R.; Mets, U. *J. Fluoresc.* **1994**, *4*, 255.
(27) Hawkins, M. E.; Pfleiderer, W.; Balis, F. M.; Porter, D.; Knutson, J. R. *Anal. Biochem.* **1997**, *244*, 86.